Applied Catalysis B: Environmental 160–161 (2014) 641–650

Contents lists available at ScienceDirect

Applied Catalysis B: Environmental

journal homepage: www.elsevier.com/locate/apcatb

Effect of preparation of iron-infiltrated activated carbon catalysts on nitrogen oxide conversion at low temperature

Martin Busch[a,b,e], Wolfgang Schmidt[f], Vadim Migunov[c,e], Andreas Beckel[d,e], Christian Notthoff[b,e], Alexander Kompch[b,e], Ulf Bergmann[a,e,*], Markus Winterer[b,e], Burak Atakan[a,e]

[a] Thermodynamics, Faculty of Engineering, University Duisburg-Essen, Lotharstrasse 1, 47057 Duisburg, Germany
[b] Nanoparticle Process Technology, Faculty of Engineering, University Duisburg-Essen, 47057 Duisburg, Germany
[c] Experimental Physics, Faculty of Physics, University Duisburg-Essen, 47057 Duisburg, Germany
[d] Solid State Physics, Faculty of Physics, University Duisburg-Essen, 47057 Duisburg, Germany
[e] Center for Nanointegration Duisburg-Essen, CENIDE, Duisburg, 47057 Duisburg, Germany
[f] Max-Planck-Institut für Kohlenforschung, 45470 Mülheim an der Ruhr, Germany

ARTICLE INFO

Article history:
Received 31 January 2014
Received in revised form 3 May 2014
Accepted 5 May 2014
Available online 13 May 2014

Keywords:
NO_x decomposition
Activated carbon
Chemical vapor infiltration
Incipient wetness method
Low temperature catalysis

ABSTRACT

Nitrogen oxides are toxic and their concentration in human workspace should be reduced to a minimum level. Among the possible catalyst materials activated carbon based catalysts are a cheap and non-toxic alternative of high availability. In this paper we investigate two different methods for the preparation of iron-infiltrated activated carbon catalysts: chemical vapor infiltration (CVI) and the incipient wetness method (IWM). The effects of the preparation method on the structure and catalytical performance are compared with the effects of infiltration load and co-deposition of silicon dioxide. The study elucidates profound differences in the nitrogen dioxide adsorption and catalytic nitrogen oxide decomposition, depending on the catalyst preparation technique. Samples prepared by chemical vapor infiltration exhibit well dispersed iron/iron oxide particles all over the sample cross section. Crystalline iron oxide is only detected in the samples prepared via the gas phase and not in samples prepared by IWM. The nitrogen dioxide adsorption is notably enhanced in samples with a large accessible micropore volume. All samples containing iron catalyze the conversion of nitrogen oxides into nitrous oxide and carbon monoxide, but especially the co-deposition of silica enhances the nitric oxide conversion into less harmful species. The iron/silica-co-deposited activated carbon catalyst prepared via incipient wetness method exhibits the best catalytical performance of all investigated catalysts at 425 K.

1. Introduction

More than 90% of nitrogen oxide (NO_x) emissions from fossil fuel power units are nitric oxide, but in the atmosphere nitric oxide is quickly oxidized to nitrogen dioxide [1]. Nitrogen dioxide however, is even more harmful than nitric oxide [2] and hence the removal of any NO_x in human workspace is of strong interest. Catalytic removal of nitrogen oxides by existing air filters would be a great progress. Since common filter materials already apply activated carbons, a modification of these seems favorable.

Carbonaceous materials like activated carbons (AC) have a long history in the technical nitrogen oxide decomposition [3,4]. Several mechanisms for the conversion reaction have been proposed [5–9] and a good overview is provided by Gao et al. [10]. Unsaturated carbon surface atoms or highly basic edge sites typically serve as reactive sites [11]. Even if a small quantity of carbon may be consumed during the reaction, the application of solid carbon as a reducing agent is probably less harmful than the possible spill of ammonia or hydrocarbons, especially in human workspace [1,12]. Furthermore, the working temperature of activated carbon based catalysts can be considerably lower than required in the efficient selective catalytic reaction (SCR) with ammonia [13,14].

Bashkova and Bandosz investigated the adsorption of nitrogen dioxide on iron-containing polymer-based porous carbons [15]. They found that the retention of nitrogen dioxide at room

Abbreviations: AC, activated carbon; CVI, chemical vapor infiltration; FIB, focused ion beam; IWM, incipient wetness method; TGA, thermal gravimetric analysis.

* Corresponding author at: Thermodynamics, Faculty of Engineering, University Duisburg-Essen, Lotharstrasse 1, 47057 Duisburg, Germany. Tel.: +49 203 3793354.
E-mail addresses: m.busch@uni-due.de (M. Busch), ulf.bergmann@uni-due.de (U. Bergmann).

http://dx.doi.org/10.1016/j.apcatb.2014.05.010
0926-3373/

temperature is a function of the pore volume, of the degree of the iron-containing particle dispersion and of the sort of predominant iron-containing species. Additionally, the NO_2 retention is highly influenced by the chemical composition of the adsorbent and by the presence of water, possibly involving a variety of surface complexes of present carbonaceous or inorganic phases [2,6,10,16].

At room temperature a significant amount of the supplied nitrogen dioxide is adsorbed by activated carbon and reduced to nitric oxide [17]. The observed increasing acidity of the sorbent is possibly caused by the formation of nitric or nitrous acid and this effect even further increases in presence of water.

Zhang et al. studied the reaction of nitrogen dioxide with activated carbons between room temperature and 423 K [7]. They suggest that nitrogen dioxide would initially oxidize the carbon surface and is simultaneously reduced to nitric oxide, which either remains chemisorbed at the carbon surface or is released to the gas phase. However, as the carbon surface becomes progressively oxidized, the rate of nitrogen dioxide conversion is significantly decreasing.

The deposition of various transition metals has been evaluated in its activity for NO_x conversion [18,19] and iron has been identified to be one of the most promising candidates [15,20,21]. The adsorption of nitrogen dioxide can be closely related of the content of metal in the carbon material, as observed for carbonaceous adsorbents containing silver nanoparticles [22]. The adsorbed nitrogen dioxide is further converted to nitric oxide, nitrous oxide, oxygen or is retained on the carbon surface by interaction with the metallic phases, e.g. by formation of chelate complexes.

In addition to the catalytic effect of the metal and carbonaceous phases, the effective size of the micropores in activated carbons seems also to have an important influence on the adsorption [10] as well as on the catalytic properties of the material [23]. However, much less research has been directed on the effect of the preparation method itself, although such a comparison can uncover profound differences in the catalytic reaction [24].

In the present work we compare for the first time the catalytic activity of four different inexpensive activated carbon based catalysts, prepared by deposition of iron or iron oxide clusters and silica inside the matrix. Two different preparation methods are applied for direct comparison: chemical vapor infiltration (CVI) and the incipient wetness method (IWM). The samples from either method are likely to differ structurally and chemically and probably differ in their catalytic activity [24]. The chosen chemical vapor infiltration process comprises two main steps: (1) homogeneous infiltration of the porous sample matrix and (2) subsequent precursor decomposition. The homogeneous sample infiltration from an alternatively applicable continuous precursor flow [25–27] is probably more difficult to control in such complex pore systems and is likely to decrease the deposition rate and precursor efficiency [28].

In addition to differences caused by the preparation method, effects of the extent of the infiltration and of the co-deposition of silicon dioxide are also evaluated. The latter may possibly prevent the sintering of adjacent iron oxide particles and stabilize the catalyst surface [29].

The infiltration homogeneity is investigated by (high resolution) transmission electron microscopy (TEM/HRTEM) from thin catalyst lamellas that have been extracted using a focused gallium ion beam (FIB). Surface structure changes during the synthesis and catalysis process are analyzed by scanning electron microscopy (SEM), X-ray diffraction (XRD) and nitrogen adsorption. The catalytic activity of the modified activated carbons is investigated by nitrogen dioxide adsorption in a thermal balance system and in a recycle flow reactor applying 0.9 mol-% NO_2 at 425 K and 100 kPa for 120 min. The experimental temperature is chosen above room temperature, in order to obtain reasonable conversion yields within a few hours.

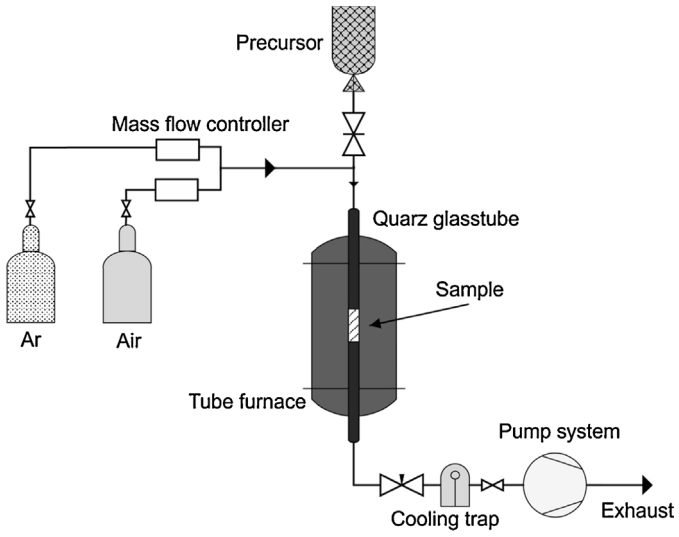

Fig. 1. Chemical vapor infiltration setup.

The catalytic effects of the samples are compared to those of iron oxide powder and of a commercial platinum reference catalyst.

2. Experimental

2.1. Catalyst preparation

Two different activated carbon materials are used as substrate materials: spherical activated carbon particles (Rütgers/CarboTech R1407, 1604 m^2/g surface area, 0.67 cm^3/g pore volume, ca. 0.5 mm particle diameter) and a commercial spherical silica adsorbent containing 14 wt.-% of activated carbon (BASF EnviSorb B+, 762 m^2/g surface area, 0.69 cm^3/g pore volume, 3–5 mm particle diameter). The applied artificially activated carbon obtains no considerable amount of impurities, which has been pre-investigated by EDX. Due to the small particle size any gas transfer limitations during the catalysis experiment are unlikely [30,31]. A low pressure reactor (Fig. 1) is used for the sample preparation [21].

The substrate is placed in a vertical quartz glass reactor tube (1.1 m long, 17 mm inner diameter) and fixed by a glass frit in the center of the tube. The reactor tube is placed inside a tube furnace (Gero F70-500/13-3, 3 heating zones) and connected to a vacuum pump system (turbo molecular pump Pfeiffer Vacuum HiPace80 and membrane pump Pfeiffer Vacuum MVP 015-4). The actual reactor volume is about 300 cm^3. The precursor supply unit at the upper end of the reactor tube consists of a lockable steel tube which is connected via a gate valve to the reactor tube. During the actual preconditioning process the precursor supply unit is kept close in an evacuated state. Upon opening of the gate valve, the porous glass container with the precursor falls down into the reactor glass tube right onto the preconditioned substrate and the precursor is ready to evaporate.

The chemical vapor infiltration preparation comprises the following steps:

1st step: Preconditioning of the substrate at less than 0.1 mbar and 573 K for 3 h.
2nd step: Evaporation of the precursor (Ferrocene ($Fe(C_5H_5)_2$), 98%, Sigma–Aldrich Inc., CAS: 102-54-5) and deposition on the sample at 0.1–10 mbar, 403 K for 2 h.
3rd step: Isobaric cooling of the sample to 303 K.
4th step: Isothermal pressure increase to 1000 mbar with air.
5th step: Isobaric heating to 653 K, heating rate 10 K/min.

The alternative preparation of activated carbons is performed by the incipient wetness method. The substrate is impregnated with solution as precursor, which is subsequently thermally decomposed to form iron(III) oxide. One of the samples is co-impregnated with 1 wt.-% silicon oxide by pre-impregnation with tetraethoxysilane (TEOS). The amounts of iron nitrate that are used for both types of impregnated materials are chosen in a way that the resulting activated carbons contain 5 wt.-% of iron oxide.

The infiltration via incipient wetness impregnation comprises the following steps:

1st step: 15 g activated carbon are impregnated with 10 mL 1 mol iron(III) nitrate solution (stirred in closed PP bottle for 5 min)
2nd step: Drying the impregnated carbon at 363 K for 16 h
3rd step: Heating the dried sample with 4 K/min to 523 K and keeping temperature for 30 min for decomposition of the iron(III) nitrate

For co-infiltration with silicon oxide the procedure was modified as follows:

1st step: 15 g activated carbon is impregnated with 10 mL of a 0.26 mol solution of TEOS in ethanol (cooled with ice bath to avoid alcohol evaporation and stirred in sealed PP bottle for 5 min)
2nd step: Heating the impregnated carbon with 4 K/min to 623 K and keeping temperature for 30 min for decomposition of the TEOS
3rd step: 15 g SiO_2 impregnated carbon is impregnated with 10 mL 1 mol iron(III) nitrate solution (stirred in closed PP bottle for 5 min)
4th step: Drying the impregnated carbon at 363 K for 16 h
5th step: Heating the dried sample with 4 K/min to 523 K and keeping temperature for 30 min for decomposition of the iron(III) nitrate

2.2. Catalyst characterization

The specific surface area is investigated by means of 77 K nitrogen adsorption (Quantachrome Autosorb 1C) using the BET method (0.01–0.1 P/P_0 for microporous samples). The pore size distribution is calculated by means of an integrated non-local density functional theory (NLDFT) software module [32]. Total pore volume data are derived from the cumulative pore volume distribution. The stated micropore volumes are derived according to the α_s-method. The data are based on the sample mass of the non-infiltrated sample.

Information on deposited iron (oxide) crystallite phases are obtained by X-ray diffraction (Panalytical X'Pert Pro MPD using Cu Kα radiation). The measurements are performed in a 2θ range of 15–85° by mounting the sample on a spinning stage and using a diffracted beam monochromator.

A dual beam FIB/SEM microscope (FEI Helios Nanolab) is used to investigate the cross section of the iron-infiltrated material. First, the spherical particle is cut into two hemispheres by a scalpel. Then, 10 μm deep trenches are milled into the cross section by means of a focused gallium ion beam, uncovering three sample pieces of 10 μm × 10 μm × 3 μm each [33]. Details on the procedure are provided as supplementary data. A micro manipulator is attached to a sample by deposition of platinum via a precursor gas. The base of the sample is then cut by the FIB and the remaining lamella is attached to a copper lift-out grid using platinum deposition. In the final step, the short side of each lamella is thinned to 100 nm with a decreased FIB current to reduce gallium implantation.

SEM micrographs are acquired from the as-deposited sample at 15 kV using a JEOL JSM 7500F microscope. Energy-dispersive X-ray spectroscopy scans are recorded in the same instrument. Investigation by high resolution transmission electron microscopy (HRTEM) is performed in a FEI Tecnai F20 instrument operating at 200 kV in bright field mode.

2.3. NO_x uptake and conversion

The NO_x uptake measurements are performed in a thermal gravimetric analysis (TGA) instrument (Bähr Thermoanalyse GmbH, STA 503) exposing 10 mg of the sample to a concentration of 0.3% nitrogen dioxide in helium gas stream of 10 sccm for 24 h at 298 K. Prior to the measurement, samples are dried in pure helium gas flow at 423 K for 1 h. The iron oxide content of the as-synthesized samples is determined by thermal gasification of all carbon in the thermal balance system at 830 K in air. At this temperature any mass loss contribution of vaporizing iron oxide should be negligible [34]. The contribution of additionally incorporated oxygen due to the possible phase change of magnetite into hematite [35] is considered to be small compared with the mass loss of carbon.

Low catalytic reaction rates are expected and thus an appropriate experimental set-up is chosen: a recycle reactor with mass spectrometric gas phase species detection. The measurement of the temperature-resolved catalytic activity is performed by surveillance of a test gas mixture (0.9 mol-% NO_2, 10 mol-% Ar, 89.1 mol-% He) at ambient pressure in this recycle flow reactor with an attached quadrupole mass spectrometer (Pfeiffer Vacuum QMS 200 with Quadstar software). The setup and measurement routine has been described elsewhere [21]. The signal intensities are normalized to argon and fitted to data of previous calibration measurements in order to derive quantitative gas phase mole fractions. Prior to the catalytic evaluation, each sample is preconditioned at 473 K in vacuum for 2 h in order to remove any physisorbed species from the carbon surface.

The activity of the synthesized catalysts is compared to a commercial platinum catalyst (5 wt.-% platinum on alumina powder, reduced, Alfa Aesar, LOT: F02R004) and to pure magnetite powder (Iron-II,III-oxide, black (magnetite), min. 95%, STREM Chemicals, CAS: 1317-61-9, surface area: 8.4 m^2/g). In order to provide fairly equal catalytically active surface areas for all measurements, the surface area of 0.3 g magnetite is estimated to match with 0.2 g of activated carbon samples. Table 1 provides an overview of all investigated samples.

3. Results and discussion

3.1. Catalyst composition and structure

The sample preparation by chemical vapor infiltration as compared to the incipient wetness method can produce very different results in the structure of the catalyst and largely affect its catalytic performance [24]. One main concern is the homogeneity of the infiltration throughout the sample and the dispersion of the deposited, catalytically active particles. Fig. 2 shows a SEM micrograph of the cross section of the iron-loaded gas phase infiltrated sample (Fe–AC–CVI). For this investigation, the sample pellet has been split into two hemispheres by using a scalpel. Iron/iron oxide clusters are identified by their contrast (bright spots). However, EDX mapping indicates a homogeneous dispersion of iron all over the entire cross section of the cut pellets (Fig. 3). EDX mapping of the cross section of the impregnated sample (Fe–AC–IWM, not shown) also reveals homogeneous iron dispersion all across the sample.

For a more detailed analysis, three lamellas, one close to the surface, one at intermediate depth and one in the center of a gas phase infiltrated activated carbon sample (Fe–AC–CVI) are extracted from the cross section of a cut sample pellet hemisphere by a focused ion beam. The cross section of the as-synthesized

Table 1
Overview of investigated samples.

Sample name	Ion exchange method	Precursor	Iron oxide/ash content (wt.-%)	Specific surface area (m^2/g)	Micropore volume (cm^3/g)
R1407-substrates					
Original AC	–	–	0.5[a]	1604	0.19
Fe–AC–IWM	IWM	$Fe(NO_3)_3$	5.8[a]	1714	0.22
Fe–AC–CVI	CVI	Ferrocene	4.7	1667	0.21
Fe–AC–CVI-13%	CVI	Ferrocene	13.0[a]	976	0.12
Fe–SiO_2–AC–IWM	IWM	$Fe(NO_3)_3/Si(OC_2H5)_4$	≈5[b]	1737	0.23
Envisorb B+ substrates					
Original Envisorb	–	–	–	776	0.15[e]
Fe–Envisorb–CVI	CVI	Ferrocene	3.4[c]	577	0.10[e]
Reference catalysts					
Pt/Al_2O_3	–	–	4.0[d]	144	–
Magnetite	–	–	–	8	–

CVI = chemical vapor infiltration, IWM = incipient wetness method.
[a] Measured by carbon gasification in TGA.
[b] Estimated from IWM.
[c] Mass gain during CVI.
[d] Quantified by EDX.
[e] Derived from NLDFT.

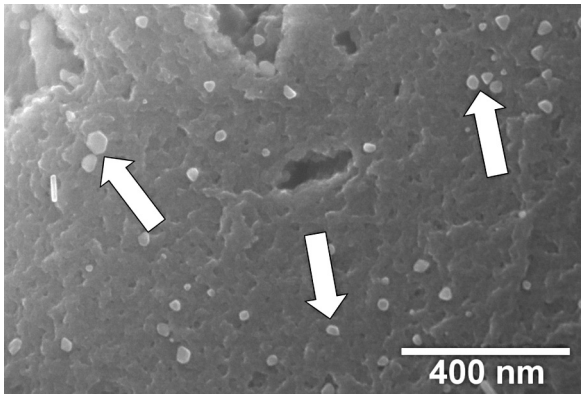

Fig. 2. SEM micrograph of Fe–AC–CVI in cut cross section with iron/iron oxide clusters (arrows) embedded in the carbon matrix.

sample is presented as supplementary data (Fig. 17), showing the extraction sites (compare to Fig. 16). The TEM images of the lamellas reveal particles of 30–50 nm diameter in macro- and mesopores, which are actually scarce in the material, as well as 2–3 nm particles dispersed all over the carbon matrix in all three lamellas (Figs. 4, 5 and 7).

In the center of the sample the concentration of visible agglomerates is slightly smaller. At intermediate depth of the sample small particles are found on the surface of larger clusters in macropores (Fig. 6). The particle contrast in HRTEM investigation, subsequent

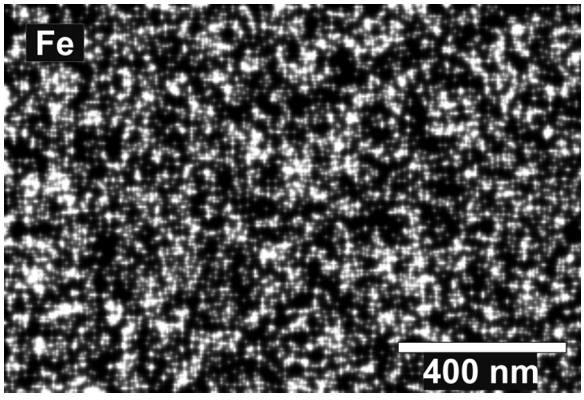

Fig. 3. EDX map of the activated carbon cut cross section of Fig. 11 showing the homogeneous dispersion of iron (bright spots).

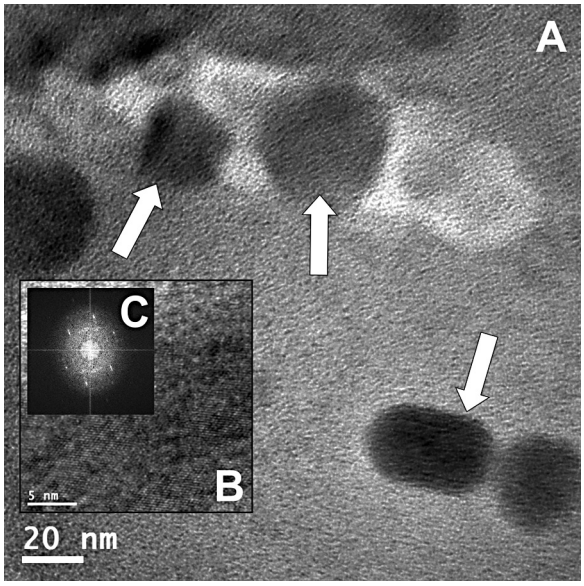

Fig. 4. TEM micrograph (A) of the sample cross section showing iron/iron oxide clusters (arrows) close to the surface of Fe–AC–CVI and HRTEM micrograph (B) of one of the larger iron/iron oxide particles with FFT of the HRTEM micrograph (C).

EDX and fast-Fourier transform (FFT) of particles close to the surface (Fig. 5) suggest that at least the larger particles consist of a metallic core and an oxidized shell of magnetite or maghemite.

The X-ray diffractograms of the synthesized samples (Fig. 8) prove the formation of crystalline magnetite/maghemite and metallic iron clusters. The largest crystallites are found in the highly iron-loaded sample Fe–AC–CVI-13%. In this sample the average magnetite/maghemite particle size – estimated by means of the Scherrer equation at the 35.5° 2θ single Bragg reflection peak is 17–19 nm, which is still detected after the NO_x catalysis experiment.

In the moderately iron-loaded gas phase infiltrated sample (Fe–AC–CVI) the average magnetite/maghemite particle size is 11 nm, approximately preserving this size during the catalysis. Due to the large peak broadening from iron oxide particles in the impregnated sample, the average crystallite size of this sample is – if present at all – below 2 nm.

Metallic iron crystallites are observed in all infiltrated samples. The characteristic reflection peak at 44.7° 2θ is superposed by a broad reflection from carbon. The estimated average size of

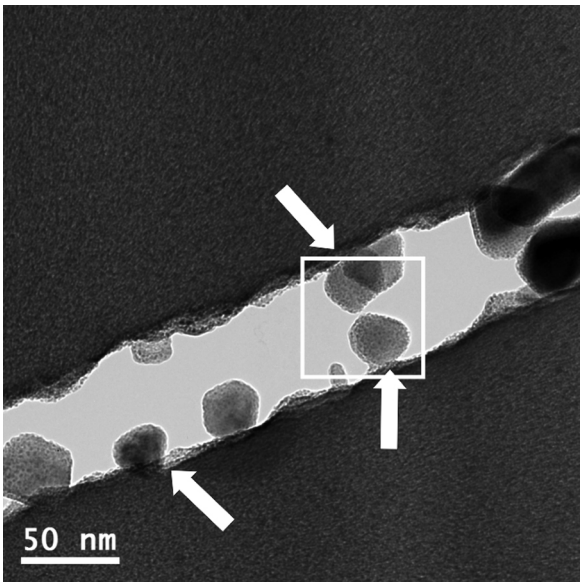

Fig. 5. TEM micrograph of the sample cross section showing iron/iron oxide clusters (arrows) inside of a large mesopore at intermediate depth of Fe–AC–CVI; the area framed white is enlarged in Fig. 15.

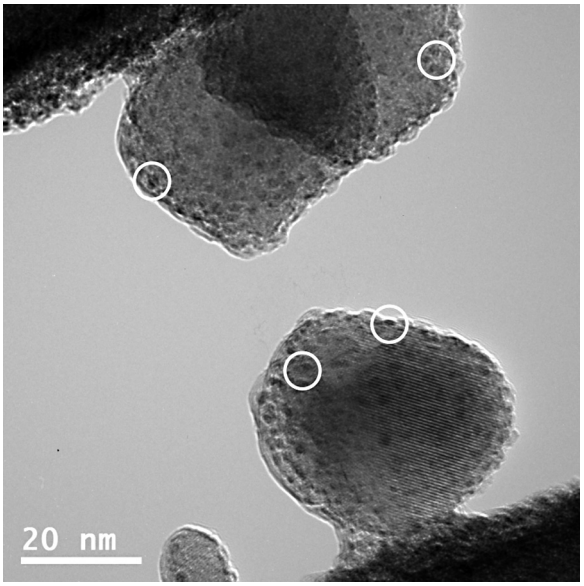

Fig. 6. TEM micrograph of the sample cross section showing small particles (white circles) on the surface of larger iron/iron oxide clusters at intermediate depth of Fe–AC–CVI, enlarged from Fig. 14.

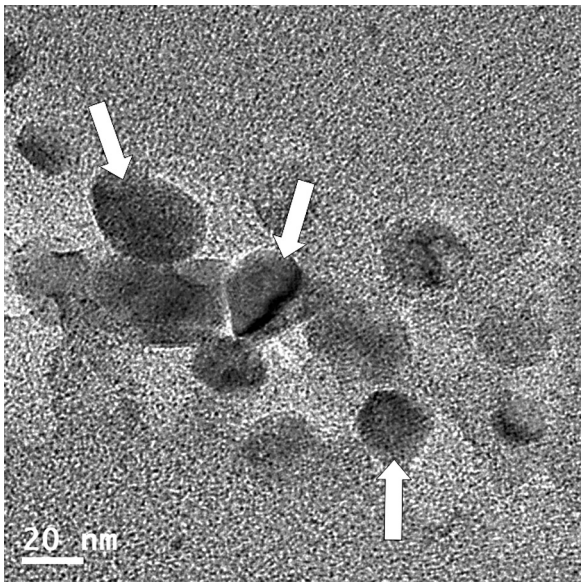

Fig. 7. TEM micrograph of the sample cross section showing iron/iron oxide clusters (arrows) in carbon matrix in the center of Fe–AC–CVI.

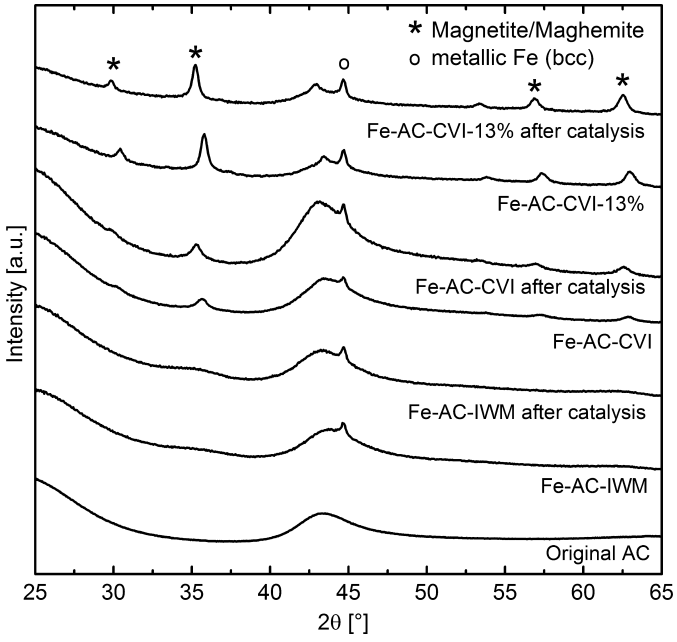

Fig. 8. X-ray diffractograms of activated carbon samples.

iron particles in the moderately iron-loaded sample (Fe–AC–CVI) is about 20 nm. The highly loaded Fe–AC–CVI-13% exhibits slightly larger iron crystallites of about 26 nm and the average size of crystallites in the impregnated sample is 24 nm, which is consistent with the SEM images.

Obviously, the main difference of impregnated and gas phase infiltrated samples is the formation of iron oxide crystallites in the samples prepared via gas phase. The reason for these findings is probably a larger quantity of oxygen available to the vapor infiltrated samples during the calcination step.

3.1.1. Kinetics of the gas-phase infiltration (CVI)

As experienced from preliminary experiments, the homogeneous infiltration of the activated carbon particles via gas phase is a challenge. Firstly, a large fraction of the Ferrocene needs to be trapped inside of the carbon matrix, and the homogenous dispersion inside of the matrix is not granted. Secondly, the Ferrocene is intended to decompose inside of the pores without excessively diffusing out of the pores during the heating to the decomposition temperature of 653 K. Even if assuming a homogenous Ferrocene adsorption throughout the pore system, the fast diffusion would probably cause a deposition gradient from the center to the border of the primary particle.

In fact, a large Ferrocene fraction of at least 75% is trapped in the pore system during the infiltration procedure. This can be roughly estimated from the mass of residual Ferrocene condensed in crystals at the cold parts of the reactor tube wall after the infiltration. A long Ferrocene evaporation time – 2 h at 403 K – is intended to promote diffusion and ensure smooth precursor dispersion inside the matrix.

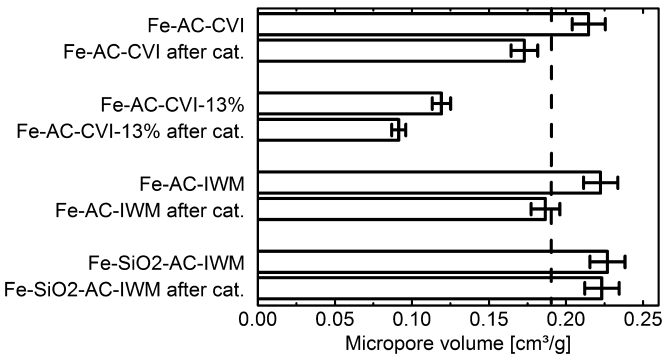

Fig. 9. Change of the specific micropore volume during the synthesis and catalysis process; the dashed line marks the micropore volume of the non-infiltrated activated carbon; cat. = catalysis experiment.

Regarding the second challenge, the reaction rate of the decomposition is required to be considerably larger than the effective diffusion of desorbing Ferrocene molecules. One possible estimate for the character of this process can be a modification of the Thiele modulus, which is commonly applied for heterogeneous catalysts [36,37].

The Thiele moduli of possible reactions suggest that the applied chemical vapor infiltration technique provides a homogeneous infiltration of the activated carbon samples as a consequence of a diffusion controlled precursor decomposition regime (for details see supplementary data). Some of the deposited larger clusters bear smaller particles, possibly indicating gas phase reactions during the Ferrocene decomposition.

3.2. Micropore analysis

Activated carbons in preparation and catalysis can be a 'vivid' system [38,39]. The structure and chemistry of the active surface and micropores are likely to change and can alternate their catalytic properties. Fig. 9 shows the change of the specific micropore volume during the sample preparation and catalysis process. After infiltration of moderate iron oxide loads (Fe–AC–CVI and Fe–AC–IWM) the specific micropore volume is slightly increased. During the catalysis process the accessible micropore volume in these samples decreases notably. The infiltration of a high load of iron (Fe–AC–CVI-13%) obviously blocks a considerable amount of the micropores which is even enforced during the catalysis process.

The actual evolution of the pore size distribution in the micropore region is shown in Fig. 10. In comparison with the micropore volume the pore volumes in the large mesopore and macropore region (not shown) are negligible, although the large pores are easily found in the TEM inspection (e.g. Fig. 5). The pore width mode is between 7 and 8 Å for all samples and the pore size distribution is not shifted during the synthesis and catalysis process. A moderate iron infiltration via gas phase (Fe–AC–CVI) results in the filling of micropores, especially at the mode width. Large iron-infiltration (Fe–AC–CVI-13%) causes a blockage of micropores in general.

The infiltration does not significantly affect the pore size distribution in case of the impregnated samples (Fe–AC–IWM). However, pores with 9 Å pore width seem to be selectively clogged. For the highly loaded Fe–AC–CVI-13% micropores decrease at all pore widths during the catalysis process. For the moderately loaded Fe–AC–CVI there is a slight increase in the narrow mesopore region. The silica-enforced sample (Fe–SiO_2–AC–IWM) is the only one without any notable change during the infiltration and catalysis.

Thermal and chemical treatments obviously induce a structural change to the pore surface. Thermal treatment of carbons may remove edge atoms and surface imperfections [31], thus decreasing the surface area and the number of reactive sites. Long evacuation times and evacuation at high temperature may lead to a detachment or decomposition of surface functional groups. Derived from Fig. 9, the thermal and chemical treatment of the infiltration procedure probably enlarges ultramicropores and makes them accessible for nitrogen adsorption at 77 K [40].

At larger infiltration levels and in the Envisorb sample the pore filling effect probably dominates and causes a drop in the measured micropore volume. This effect is also observed by other authors for silver-infiltrated activated carbon samples [22]. An increased silver-load results in clogging especially of small mesopores.

During the NO_x decomposition process unsaturated carbon atoms at high energy sites are likely to be oxidized and may desorb in form of carbon oxides as will be discussed further below. Gasification, especially of thin carbon walls that separate neighboring pores, may cause a merging of these pores. This effect is probably observed for the moderately infiltrated sample Fe–AC–CVI. The reported pore-width selective chemisorption of nitric oxide [41–43] can be responsible for the large pore volume decrease at 9 Å pore width. The co-deposition of silica (Fe–SiO_2–AC–IWM) obviously prevents such pore clogging. It may be speculated that the deposition of silica may hamper the reported sintering of catalyst particles [44], thus keeping the pores well accessible, but the actual effects still need to be investigated.

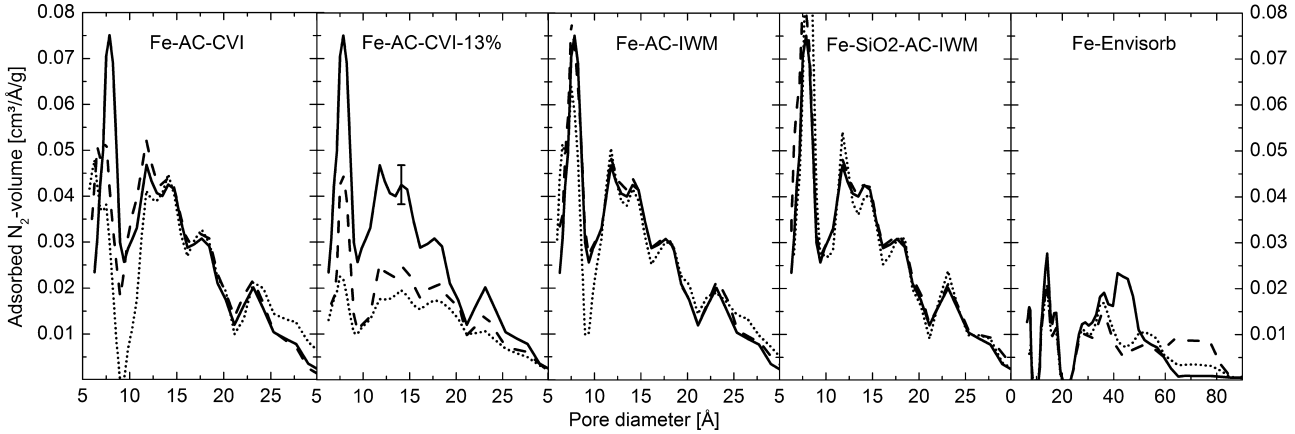

Fig. 10. Micropore size distribution of activated carbon samples and Envisorb; solid line: non-infiltrated matrix material, dashed line: infiltrated sample, dotted line: infiltrated sample after catalysis experiment, exemplary error bar.

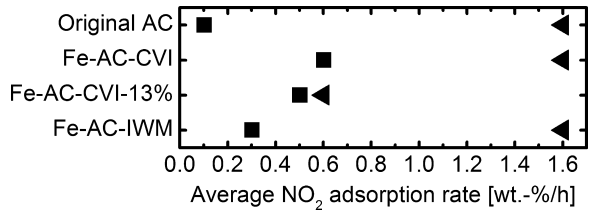

Fig. 11. Average NO_2 adsorption rate during the first 10 h (triangles) and last 4 h (squares) of the 24 h NO_2 adsorption experiments.

3.3. NO_x uptake capability

Especially due to their large quantity of micropores, activated carbons are well known to exhibit excellent adsorption properties for many gases. The adsorption capacity of nitrogen oxides could serve as a good indicator for the ability of the synthesized material to trap these harmful species from the ambient air at human workspace, even if the actual conversion kinetics may be slow. In a thermal balance instrument 10 mg of an activated carbon sample are exposed to 0.3% nitrogen dioxide in helium gas stream for 24 h at 298 K. It has to be noted, that the maximum uptake capability is not exhausted during this time, except of the non-infiltrated sample.

The investigation, which is presented in detail as supplementary data, shows that the non-infiltrated and the impregnated samples (Original AC and Fe–AC–IWM) exhibit similar nitrogen dioxide uptake, while the gas phase infiltrated sample (Fe–AC–CVI) shows a significantly larger uptake.

Fig. 11 compares the average rates of the nitrogen dioxide adsorption per hour during the first 10 h and during the last 4 h of the described 24 h adsorption experiment. Initially, all activated carbon samples, except of the highly infiltrated Fe–AC–CVI-13%, exhibit the same adsorption rate of 1.6 wt.-%/h. Closer to sample saturation the adsorption rates decrease, but remain larger for the gas phase infiltrated samples (about 0.6 wt.-%/h) than for the impregnated and the non-infiltrated sample. The non-infiltrated activated carbon is completely saturated with nitrogen dioxide after 14 h, while the infiltrated samples do not reach complete saturation in the experiment time. The greatest nitrogen dioxide uptake (26 wt.-%) is observed for the gas phase infiltrated Fe–AC–CVI (see Fig. 19, supplementary data).

As observed for the highly infiltrated Fe–AC–CVI-13%, the clogging of micropores may limit the nitrogen dioxide uptake [44,45]. For the samples with similar micropore volume (Original AC, Fe–AC–CVI and Fe–AC–IWM), the pore width mode is probably more important than the actual pore volume for the nitrogen dioxide uptake [41,42] as well as for a possible nitric oxide conversion [10,23]. In the direct comparison of samples with similar infiltration load and similar pore size distribution (Fe–AC–CVI and Fe–AC–IWM), the gas phase infiltrated sample performs slightly better in the adsorption of nitrogen dioxide than the impregnated sample.

In summary, the nitrogen dioxide uptake is significantly enhanced for the sample infiltrated via CVI. A high infiltration load limits the uptake, probably due to micropore clogging. Infiltration via incipient wetness method does not increase the uptake capability compared to the original sample, though the impregnated sample is not yet saturated at the end of the experiment.

3.4. Nitrogen dioxide decomposition

Being one of the most harmful pollutants, the complete decomposition of nitrogen oxides in human workspace is a preferential goal. In typical conditions of human workspace, i.e. temperatures close to ambient and with avoidance of any harmful additives, intermediate reaction products may be formed and a considerable amount of the reaction educts or products may remain adsorbed on the catalyst. In the applied recycle flow reactor at 425 K such conditions are simulated. The synthesized catalysts are exposed to an initial gas mixture of 0.9 mol-% nitrogen dioxide, 10 mol-% argon and 89.1 mol-% helium for 120 min. For the sake of monitoring kinetically slow reactions in very effective NO_x adsorbants, the applied concentration of nitrogen dioxide is larger than what would be expected in a typical workspace environment. Fig. 12 shows the final gas composition of all investigated samples after 120 min experiment time.

The platinum reference catalyst adsorbs all nitrogen dioxide without notable desorption of any reaction products, except of a small quantity of nitric oxide. Magnetite adsorbs half of the nitrogen dioxide and releases some molecular nitrogen and molecular oxygen, but the largest part of nitrogen dioxide remains un-converted. In contrast, all carbon-based catalysts convert nitrogen dioxide almost completely to nitric oxide, nitrous oxide, carbon monoxide and a small quantity of carbon dioxide.

The iron-infiltrated activated carbon catalysts produce more nitrous oxide and carbon monoxide than the non-infiltrated activated carbon. The co-deposition of silica induces an increasing nitrous oxide release and slightly more carbon monoxide. The release of pure oxygen or pure nitrogen is not observed for the carbon samples. Iron-infiltrated Envisorb exhibits a larger activity in the conversion of nitrogen dioxide into nitrous oxide, carbon monoxide and carbon dioxide than the non-infiltrated Envisorb.

Fig. 13 shows the change of the applied gas mixture composition (0.9 mol-% NO_2, 10 mol-% Ar, 89.1 mol-% He) in detail during the first 90 s of the experiment at 425 K. All activated carbon samples quickly adsorb and reduce nitrogen dioxide. The fastest nitrogen dioxide conversion is detected for the non-infiltrated activated carbon (Original AC) and the impregnated samples (Fe–AC–IWM and Fe–SiO_2–AC–IWM). The largest part of nitrogen dioxide is immediately converted into nitric oxide and – to a smaller extent – into equimolar mole fractions of carbon monoxide and nitrous oxide. For the unmodified activated carbon sample (Original AC) the nitric oxide desorption after 90 s is considerably higher (0.7 mol-%) than for all infiltrated carbon samples (0.5 mol-%). The detected nitrogen and oxygen mole fractions (not shown) are below the impurity level (0.1 mol-%) in the gas mixture and remain constant.

The balanced sum of elements in the gas mixture is only for the unmodified activated carbon fairly equal to the initial nitrogen dioxide mole fraction. All other activated carbon samples keep approximately 15% of the initially provided nitrogen dioxide adsorbed on the sample, i.e. this fraction of nitrogen dioxide is not released to the gas phase in form of any reaction products. The nitrogen dioxide conversion is much slower for Envisorb samples. The iron-infiltrated Envisorb shows slightly faster nitrogen dioxide reduction than the non-infiltrated sample. For the Envisorb samples the adsorption of nitrogen dioxide is in elemental balance with the sum of released reaction products.

The initial mole fraction of 0.9 mol-% nitrogen dioxide is quickly decreasing, probably due to the adsorption of nitrogen dioxide in micropores [1,46]. During the subsequent reduction of nitrogen dioxide, the largest part of the resulting nitric oxide is released to the gas phase. The remaining adsorbed oxygen is most probably oxidizing the carbon or metal catalyst surface, accompanied by a possible formation of various surface complexes as reported in detail elsewhere [6,7,9].

Redox reactions involving iron oxide catalyze the NO_x reduction [15,20]. The transfer of the accumulating adsorbed oxygen atoms to the activated carbon support is considered to be rate limiting [47]. However, in the present results, the infiltration with iron does

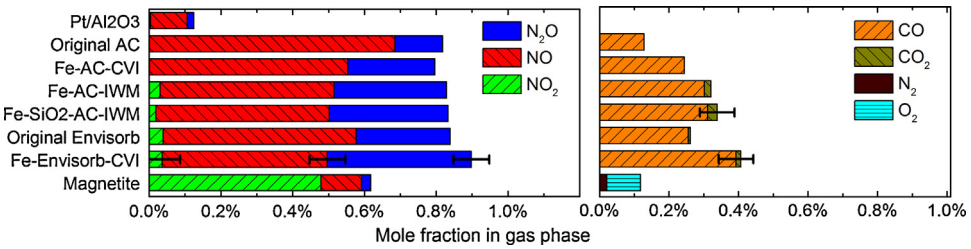

Fig. 12. Reaction products from NO_2 decomposition experiments after 120 min at 425 K with exemplary error bars (initial gas mixture: 0.9 mol-% NO_2, 10 mol-% Ar, 89.1 mol-% He).

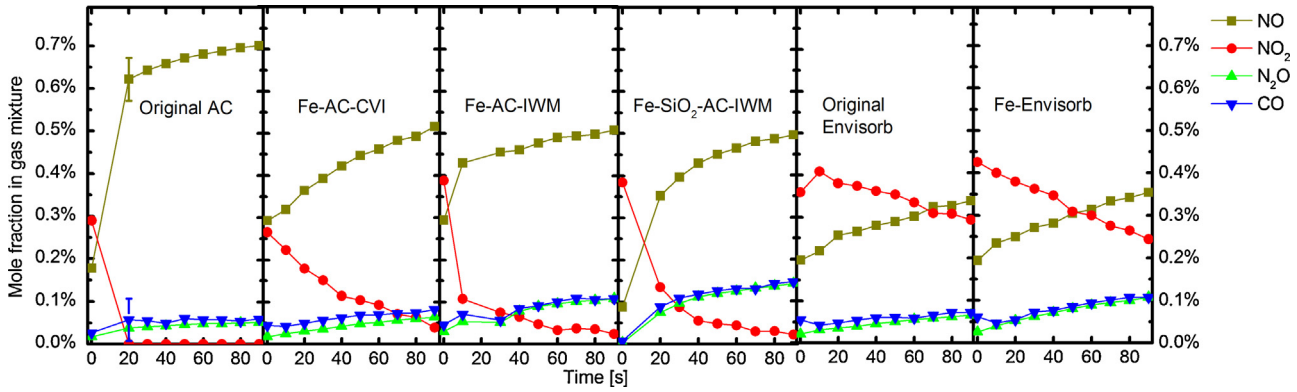

Fig. 13. Gas mixture composition during the first 90 s of adsorption and decomposition of NO_2 in recycle flow at 425 K (initial NO_2 mole fraction was 0.9 mol-%) with exemplary error bars.

not improve the initial nitrogen dioxide removal rate in comparison to the non-infiltrated activated carbon sample. Probably, the adsorptive effect of the micropores is just too dominating at this stage.

3.5. Further decomposition of nitric oxide

In the course of the catalysis experiment nitric oxide is released to the gas phase and needs to be further converted into less toxic reaction products. Fig. 14 shows the decrease of the nitric oxide mole fraction during the last 90 min of the described catalysis experiment at 425 K in recycle flow. The silica-co-deposited activated carbon (Fe–SiO_2–AC–IWM) exhibits the largest rate of nitric oxide decomposition. The unmodified Envisorb even continues to produce some nitric oxide. The largest nitric oxide conversion rates are found in samples exhibiting a large availability of micropore volume (see Table 1).

The deposited iron or iron oxide species contribute to the catalytic activity, as derived from the comparison of the Envisorb samples. Oxygen defects in the lattice of iron oxides are believed to serve as active centers in the catalytic decomposition reaction of nitrogen oxides, but the actual mechanism is likely to involve a large number of intermediate complexes [15,22,48,49].

The co-deposition of silica obviously has a very positive effect on the nitric oxide decomposition. If the transfer of oxygen to the carbon support is assumed to be rate limiting for the overall process, silica may possibly enhance the oxygen transfer. The results for Envisorb samples suggest that a lower surface area, less micropores or a lower availability of carbon may have a negative effect on the nitrogen dioxide conversion rate.

Fig. 15 shows in detail the time-resolved evolution of the test gas composition with iron/silica-infiltrated activated carbon over the entire experiment. While the nitric oxide mole fraction decreases, equimolar fractions of carbon monoxide and nitrous oxide are released and a small quantity of carbon dioxide is detected.

Gaseous nitric oxide can be adsorbed in form of C–NO complexes [50] or it is dissociated on the carbon or metal catalyst [18].

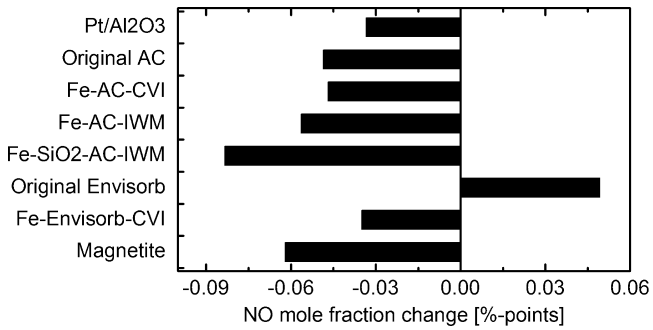

Fig. 14. Change of NO mole fraction in gas phase during the last 90 min in recycle flow at 425 K.

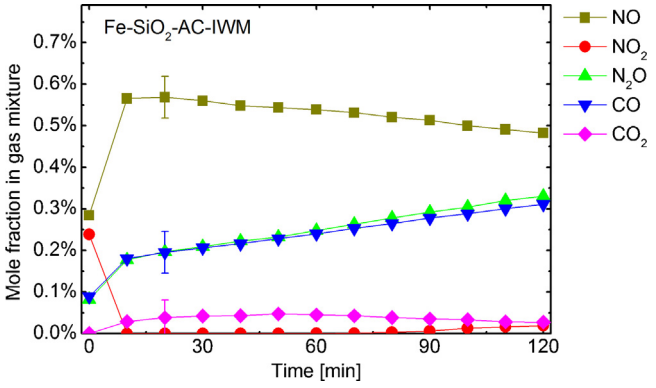

Fig. 15. Gas composition during adsorption and decomposition of NO_2 with Fe–SiO_2–AC–IWM in recycle flow reactor for 120 min (425 K, initial NO_2 mole fraction is 0.9 mol-%), exemplary error bars.

Table 2
Results of NO_2 adsorption and decomposition experiment in recycle flow after 120 min (425 K, 100 kPa); marks are derived from relative comparison among the investigated samples, details are provided as supplementary data.

Catalyst	Adsorption or decomposition of NO_2	Decomposition of NO	Content of in gas mixture					
			NO	N_2O	N_2	O_2	CO	CO_2
Pt/Al_2O_3	+++	0	0	0		–		
Original AC	+++	0	+++	+			+	–
Fe–AC–CVI	+++	0	+++	++			++	–
Fe–AC–IWM	++	+	+++	+++			++	0
Fe–SiO_2–AC	++	++	+++	+++			+++	0
Original Envisorb B+	++	–	+++	++			++	0
Fe–Envisorb B+	++	0	+++	+++			+++	0
Magnetite	–	+	0	0	0	+		

Considering the reaction mechanism proposed by Teng et al. for carbon oxides formation from nitric oxide [8], it is interesting that in the present conditions much more carbon monoxide than carbon dioxide is released and no molecular nitrogen at all. The desorption of carbon monoxide is typically observed at higher temperatures [51–53].

Hence, the present results suggest a preferred NO-adsorption in form C–NO_x or C–$(NO)_x$ complexes rather than C–N which would be a direct precursor for the not observed formation of molecular nitrogen [31]. The desorption of carbon monoxide is parallel to the desorption of nitrous oxide and is inversely parallel to the decreasing mole fraction of nitric oxide. Neighboring C–NO complexes are suggested as a possible precursor for the formation of nitrous oxide [54] and the leftover C–O may desorb in form of carbon monoxide.

The released reaction products carbon monoxide and nitrous oxide become more important over the experiment time and might participate in the reaction. Nitrous oxide can additionally compete with nitrogen dioxide for reaction sites [55,56]. At least carbon monoxide as a NO_x-reductant is not observed, since it would be associated with a significant formation of carbon dioxide [31,57].

3.6. Catalyst performance comparison

The effects from the recycle flow experiments (Fig. 12) are summarized and compared in Table 2. The underlying data and rating is provided as supplementary data. Although nitrogen dioxide in the feed gas and product nitric oxide are not completely decomposed into their elements, the conversion into nitrous oxide and carbon oxides is a huge progress. The World Health Organisation (WHO) guidelines recommend maximum acceptable indoor concentrations of nitrogen dioxide, which are by one order of magnitude lower than that of carbon monoxide [58]. There are no defined WHO guidelines for nitrous oxide, but according to the German Federal Institute for Occupational Safety and Health the acceptable workspace concentrations of nitrous oxide are by far larger than that of nitrogen dioxide [59].

Hence, the fast trapping of nitrogen oxides in the catalyst material is a helpful step before the kinetically slow conversion. Regarding this adsorption process the gas phase infiltrated catalyst Fe–AC–CVI seems preferential since it shows the largest capacity for nitrogen dioxide. The subsequent conversion of nitrogen dioxide at 425 K is observed for all investigated catalysts. However, the silica-co-deposited Fe–SiO_2–AC–IWM prepared by the incipient wetness method exhibits the best conversion performance of the intermediately produced nitric oxide during the 120 min experiment time and is considered to be the superior catalyst.

4. Summary and conclusions

In the current paper we investigate effects of the sample preparation of iron-infiltrated activated carbon catalysts on the nitrogen oxides adsorption and decomposition at low temperature. Two different preparation methods are chosen: the incipient wetness method and the chemical vapor infiltration. Additionally, the infiltration of a larger iron load and the co-deposition of silica in the sample matrix are evaluated.

The applied chemical vapor infiltration comprises two main steps: (1) homogenous infiltration of the precursor and (2) subsequent precursor decomposition. While the precursor infiltration is performed under reaction controlled conditions, a consideration of the kinetics shows that the decomposition occurs rather in a diffusion controlled regime. Samples synthesized in this way exhibit iron/iron oxide clusters well dispersed all over the carbon matrix. Some of these clusters carry smaller particles on their surface, probably stemming from secondary nucleation. At least a part of the clusters seems to consist of a metallic core and an oxidized shell.

The micropore volume of the sample is slightly increased during the infiltration procedure, probably due to an opening of pores in the thermal treatment. The pore size distribution is well preserved and the sample exhibits excellent NO_x adsorption properties. At 425 K the catalyst removes nitrogen dioxide quickly from the test gas atmosphere, releasing at first a large quantity of nitrogen monoxide. The nitrogen monoxide is further decomposed into nitrous oxide and carbon monoxide, however with much slower kinetics. During this catalytic decomposition the micropore volume of the sample is slightly decreasing.

The alternatively prepared sample via incipient wetness method shows good dispersion of the infiltrated iron, too, but no crystalline iron oxide is detected. The catalytic activity is similar to that of the gas phase infiltrated sample, releasing slightly more nitrous oxide and carbon oxides. Some micropores are blocked during the catalysis process.

The infiltration of a large iron load via the gas phase results in a strong clogging of micropores. In this case the adsorption capacity for nitrogen dioxide is significantly reduced. In contrast, the wet chemical co-deposition of silica and iron keeps the pore system well accessible during infiltration and catalysis. Hence, the Fe–SiO_2–AC–IWM is considered to be the best catalyst due to its superior conversion performance of the intermediately produced nitric oxide into the less harmful nitrous oxide and carbon oxides at 425 K. It is hence the most promising candidate for the application in human workspace.

Acknowledgments

The authors thank Mr. A. Hein, Mr. S. Suleiman, Mr. S. Lorenz, Mr. A Görnt and Mr. F. Sen for technical support. The authors would like to thank for financial support from the German Federal Ministry of Economics and Technology (Grant no. 15751N) within the agenda for the promotion of industrial cooperative research and development (IGF) based on a decision of the German Bundestag. The access was opened by the IUTA e. V., Duisburg, and organized by the (IGF-Project No. 15751N).

Appendix A. Supplementary data

Supplementary data associated with this article can be found, in the online version, at http://dx.doi.org/10.1016/j.apcatb.2014.05.010.

References

[1] J.K. Neathery, A.M. Rubel, J.M. Stencel, Carbon 35 (1997) 1321.
[2] R. Pietrzak, T.J. Bandosz, Carbon 45 (2007) 2537–2546.
[3] M.S. Shah, J. Chem. Soc. (1929) 2661–2676.
[4] M.S. Shah, J. Chem. Soc. (1929) 2676–2692.
[5] G.M. Underwood, T.M. Miller, V.H. Grassian, J. Phys. Chem. A 103 (1999) 6184–6190.
[6] M. Jeguirim, V. Tschamber, J.F. Brilhac, P. Ehrburger, J. Anal. Appl. Pyrol. 72 (2004) 171–181.
[7] W.-J. Zhang, A. Bagreev, F. Rasouli, Ind. Eng. Chem. Res. 47 (2008) 4358–4362.
[8] H. Teng, E.M. Suuberg, J.M. Calo, Energy Fuels 6 (1992) 398–406.
[9] N. Shirahama, S.H. Moon, K.H. Choi, T. Enjoji, S. Kawano, Y. Korai, M. Tanoura, I. Mochida, Carbon 40 (2002) 2605–2611.
[10] X. Gao, S. Liu, Y. Zhang, Z. Luo, M. Ni, K. Cen, Fuel Process. Technol. 92 (2011) 139–146.
[11] B. Xia, J. Phillips, C.-K. Chen, L.R. Radovic, I.F. Silva, J.A. Menendez, Energy Fuels 13 (1999) 903–906.
[12] M.J. Illán-Gómez, E. Raymundo-Pinero, A. García-García, A. Linares-Solano, C. Salinas-Martínez de Lecea, Appl. Catal. B: Environ. 20 (1999) 267–275.
[13] K. Skalska, J.S. Miller, S. Ledakowicz, Sci. Total Environ. 408 (2010) 3976–3989.
[14] G. Busca, L. Lietti, G. Ramis, F. Berti, Appl. Catal. B: Environ. 18 (1998) 1–36.
[15] S. Bashkova, T.J. Bandosz, ChemSusChem 4 (2011) 404–412.
[16] H. Muckenhuber, H. Grothe, Carbon 44 (2006) 546–559.
[17] R. Pietrzak, Energy Fuels 23 (2009) 3617–3624.
[18] M.J. Illán-Gómez, A. Linares-Solano, C. Salinas-Martinez de Lecea, Energy Fuels 9 (1995) 976–983.
[19] H. Bosch, F. Janssen, Catalytic Reduction of Nitrogen Oxides. A Review on the Fundamentals and Technology, Elsevier, Amsterdam, New York, 1988, VII p.
[20] M.J. Illán-Gómez, A. Linares-Solano, L.R. Radovic, C. Salinas-Martínez de Lecea, Energy Fuels 10 (1996) 158–168.
[21] M. Busch, U. Bergmann, U. Sager, W. Schmidt, F. Schmidt, C. Notthoff, B. Atakan, M. Winterer, J. Nanosci. Nanotechnol. 11 (2011) 7956–7961.
[22] M. Seredych, S. Bashkova, R. Pietrzak, T.J. Bandosz, Langmuir 26 (2010) 9457–9464.
[23] W.J. Zhang, S. Rabiei, A. Bagreev, M.S. Zhuang, F. Rasouli, Appl. Catal. B: Environ. 83 (2008) 63–71.
[24] A.E. Aksoylu, J.L. Faria, M.F.R. Pereira, J.L. Figueiredo, P. Serp, J.C. Hierso, R. Feurer, Y. Kihn, P. Kalck, Appl. Catal. A: Gen. 243 (2003) 357–365.
[25] Y. Sohda, R.J. Diefendorf, Extended Abstracts, 17th Biennial Conference on Carbon, American Carbon Soc, Lexinton (Kentucky, USA), 1985, pp. 31–32.
[26] Z. Hu, K.J. Hüttinger, Carbon 39 (2001) 1023–1032.
[27] W. Zhang, K.J. Hüttinger, Carbon 39 (2001) 1013–1022.
[28] P. Delhaès, in: P. Delhaès (Ed.), Fibers and Composites, CRC Press, London, 2003.
[29] B. Curdts, M. Helmich, C. Pasel, D. Bathen, B. Atakan, C. Pflitsch, Phys. Proc. 46 (2013) 248–254.
[30] S. Stegenga, R. van Soest, F. Kapteijn, J.A. Moulijn, Appl. Catal. B: Environ. 2 (1993) 257–275.
[31] I. Aarna, E.M. Suuberg, Fuel 76 (1997) 475–491.
[32] P.I. Ravikovitch, A. Vishnyakov, R. Russo, A.V. Neimark, Langmuir 16 (2000) 2311–2320.
[33] R.M. Langford, A.K. Petford-Long, J. Vacuum Sci. Technol. A 19 (2001) 2186–2193.
[34] W.M. Shchedrin, I.S. Kulikov, V.N. Vas'kin, A.A. Teleguin, J. Chem. Thermodyn. 10 (1978) 9–18.
[35] G. Ketteler, W. Weiss, W. Ranke, R. Schlogl, Phys. Chem. Chem. Phys. 3 (2001) 1114–1122.
[36] E.W. Thiele, Ind. Eng. Chem. 31 (1939) 916–920.
[37] O. Deutschmann, H. Knözinger, K. Kochloefl, T. Turek, Ullmann's Encyclopedia of Industrial Chemistry, Wiley-VCH Verlag GmbH & Co. KGaA, Weinheim, 2009.
[38] I. Menendez, A.B. Fuertes, Carbon 39 (2001) 733–740.
[39] M. Gurrath, T. Kuretzky, H.P. Boehm, L.B. Okhlopkova, A.S. Lisitsyn, V.A. Likholobov, Carbon 38 (2000) 1241–1255.
[40] K. Kakei, S. Ozeki, T. Suzuki, K. Kaneko, J. Chem. Soc. Faraday Trans. 86 (1990) 371–376.
[41] A.M. Rubel, M.L. Stewart, J.M. Stencel, J. Mater. Res. 10 (1995) 562–567.
[42] A.M. Rubel, M.L. Stewart, J.M. Stencel, ACS Symp. Ser. 587, 208–216.
[43] K. Kaneko, Langmuir 3 (1987) 357–363.
[44] M.J. Illán-Gómez, C. Salinas-Martínez de Lecea, A. Linares-Solano, L.R. Radovic, Energy Fuels 12 (1998) 1256–1264.
[45] S. Bashkova, T.J. Bandosz, Ind. Eng. Chem. Res. 48 (2009) 10884.
[46] S. Bashkova, T.J. Bandosz, J Colloid Interface Sci 333 (2009) 97–103.
[47] M.J. Illán-Gómez, A. Linares-Solano, L.R. Radovic, C. Salinas-Martinez de Lecea, Energy Fuels 9 (1995) 540–548.
[48] M. Iwamoto, H. Hamada, Catal. Today 10 (1991) 57.
[49] R. Pietrzak, T.J. Bandosz, J. Hazard. Mater. 154 (2008) 946–953.
[50] H. Teng, E.M. Suuberg, J. Phys. Chem. 97 (1993) 478–483.
[51] H. Teng, E.M. Suuberg, Ind. Eng. Chem. Res. 32 (1993) 416–423.
[52] L.K. Chan, A.F. Sarofim, J.M. Beér, Combust. Flame 52 (1983) 37–45.
[53] T. Furusawa, M. Tsunoda, M. Tsujimura, T. Adschiri, Fuel 64 (1985) 1306–1309.
[54] T. Okuhara, K.-I. Tanaka, J. Chem. Soc. Faraday Trans. 1: Phys. Chem. Condens. Phases 82 (1986) 3657–3666.
[55] J.A. Moulijn, F. Kapteijn, Carbon 33 (1995) 1155–1165.
[56] S.A. Carabineiro, F.B. Fernandes, R.J.C. Silva, J.S. Vital, A.M. Ramos, I.M. Fonseca, Catal. Today 133–135 (2008) 441–447.
[57] I. Aarna, E.M. Suuberg, Energy Fuels 13 (1999) 1145–1153.
[58] WHO, WHO Guidelines for Indoor Air Quality: Selected Pollutants, World Health Organization, Bonn, 2010.
[59] BAuA, Bundesanstalt für Arbeitsschutz und Arbeitmedizin – Ausschuss für Gefahrstoffe, Arbeitsplatzgrenzwerte Januar, 2006.
[60] Y. Maeda, N. Ogawa, Y. Takashima, J. Chem. Soc. Dalton Trans. (1987) 627–632.
[61] E. Schieferstein, S. Schlüter, T. Hennig, K. Meller, M. Lange, A. Möller, Chem. Ingenieur Tech. 85 (2013) 934–943.
[62] P.G. Gray, Gas Separat. Purif. 7 (1993) 213.
[63] P.L.J. Mayfield, D.D. Do, Ind. Eng. Chem. Res. 30 (1991) 1262–1270.
[64] G.L. Bertrand, G. Caboche, L.C. Dufour, Solid State Ionics 129 (2000) 219.
[65] J.M. Thomas, W.J. Thomas, J.R. Anderson, M. Boudart, Principles and Practice of Heterogeneous Catalysis, VCH, Weinheim, 1997.
[66] K.E. Lewis, G.P. Smith, J. Am. Chem. Soc. 106 (1984) 4650–4651.
[67] G.T. Linteris, M.D. Rumminger, V. Babushok, W. Tsang, Proc. Combust. Inst. 28 (2000) 2965–2972.
[68] K. Kuwana, K. Saito, Carbon 43 (2005) 2088.
[69] L.M. Dyagileva, V.P. Mar'in, E.I. Tsyganova, G.A. Razuvaev, J. Organometal. Chem. 175 (1979) 63–72.
[70] K. Kuwana, K. Saito, Proc. Combust. Inst. 31 (2007) 1857–1864.
[71] T. Hirasawa, C.-J. Sung, Z. Yang, A. Joshi, H. Wang, Combust. Flame 139 (2004) 288–299.